RESEARCH

Investigation of the frequency effect on electrical modulus and dielectric properties of Al/p-Si structure with %0.5 Bi:ZnO interfacial layer

S. Bengi[1] · H. G. Çetinkaya[2] · Ş. Altındal[3] · P. Durmuş[3]

Abstract

Capacitance and conductance measurements were made to evaluate the effects of voltage and frequency on the dielectric properties, ac electrical conductivity (σ_{ac}), and electric-modulus of the Al/%0.5 Bi:ZnO/p-Si structures. The measurements were taken in a voltage range of $(-4\ V)$–$(+4\ V)$ and frequency range of 0.1–1 MHz, respectively. All parameters were discovered to have substantial relationships to voltage and frequency at accumulation and depletion regions due to relaxation mechanisms and interface traps positioned between %0.5 Bi:ZnO interlayer and p-Si with energies in the Si bandgap. The e'-V, M''-V, and Z'-V plots all demonstrate a peak, and because of electronic charges being reordering and restructuring at surfaces, traps, and dipole-polarization under the external electric field, the peak's position and magnitude vary with frequency. The double logarithmic σ_{ac}-w curve shows linear behaviour, its slope was found as 0.699, and this value of the Al/%0.5 Bi:ZnO/p-Si/Au structure has high ac conductivity or low resistivity. The observed high changes in the dielectric constant and dielectric loss (e', e'') were explained by Maxwell–Wagner type polarization as well as interface traps.

Keywords %0.5 Bi:ZnO interlayer · Frequency dependence · Electric modulus · Dielectric properties · Ac electrical conductivity

Introduction

An insulator/oxide or metal oxide layer is formed in MS structures with a metal oxide layer by sandwiching an interfacial layer (e.g. HfO_2, TiO_2, Si_3N_4, SnO_2, CdO, or ZnO) between the metal and the semiconductor [1–6]. These devices are very important technically; thus, researchers are quite interested in their electrical, optical, and dielectric properties. The formation of barrier height (BH) at the junction, series resistance (Rs) of the structure, polarization, frequency, and voltage, as well as surface preparation and fabrication processes, the native and grown interfacial layer at the M-S interface, interface traps and dislocations at the interlayer/semiconductor interface, and more are all dependent upon these features [7–10]. The characteristics of BH and its homogeneities are influenced by the doping concentration of donor or acceptor atoms, frequency, temperature, applied electric field ($E = V/d$), and grain boundaries [2–5]. These factors are of great interest to the scientific community and require substantial examination to optimize the performance of MS structures with interfacial layers.

Among the metal oxide thin films, especially zinc-oxide (ZnO) is particularly attractive in this regard due to their low resistivity, cost-effectiveness, radiation resistant, non-toxicity, and high thermal/chemical stability [10–14]. Sometimes, ZnO is called a semiconductor material composed of zinc and oxygen elements, belonging to the II-VI group of the periodic table and it exhibits an n-type conductivity and possesses a hexagonal wurtzite crystal structure. In addition, both its large bandgap energy (3.37 eV) and high binding energy (at about 60 mV) make it a crucial semiconductor [10–13, 15–18]. Because of this wide optical band gap, ZnO has a good transparency in the wavelength range

✉ S. Bengi
sbengi@baskent.edu.tr

1 Vocational School of Technical Sciences, Başkent University, 06790 Ankara, Turkey

2 Vocational School of Health Services, Gazi University, 06830 Ankara, Turkey

3 Department of Physics, Faculty of Sciences, Gazi University, 06500 Ankara, Turkey

of 4000–7000 Å (VR: visible range), and hence, it has a promising material in optoelectronic applications such as photodiodes (PDS), solar cells (SCs), light-emitting diodes (LEDs), photodetectors (PDs), and MIS type Schottky diodes (SDs) [10–13].

To increase permittivity of the pure ZnO, it was doped with various metals such as Cu, Bi, Cd, Al, Mg, Mn, Ga, Co, and In have been employed as an interfacial layer at the M-S interface to enhance the performance and quality of MS type electronic devices [19–26]. Such interlayer regulates the charge transport between metal and semiconductor, prevents inter-diffusion, and isolates from each other. A thin ZnO film can be deposited using a variety of techniques, including chemical vapour deposition (CVD), the sol–gel, radio frequency magnetron sputtering (RF), and spin coating [27, 28]. The interfacial layer's development and the surface preparation parameters have a significant impact on the MIS device's electric and dielectric characteristics [29–36]. The presence of an interlayer between the semiconductor and the metal top contact can alter the diode's properties, mostly by raising the structure's barrier height. Permittivity, thickness, and homogeneity all affect capacitance and conductance values. Nonetheless, the spin coating sputtering technique was selected for this investigation due to its many benefits over alternative deposition techniques. This technique is popular since it is quicker and less expensive while producing more uniform sputtering over a wider region.

Determining the impacts of ZnO's Bi doping content was the aim of the earlier investigation. The same p-Si wafer was used to create Al/Bi:ZnO/p-Si diodes with varying weight percentages (pure, %0.1, %0.3, and %0.5). From there, measurements of their current, capacitance, and voltage under varied illumination and intensity conditions as well as in the dark were used to determine their basic electrical characteristics. According to research results, the ideal Bi doping level in ZnO is %0.5 when considering lower ideality factor and surface state values and higher barrier height and shunt resistance values [37]. Precise information on both the electric and dielectric characteristics is not provided by *C/G-V* measurements which conducted solely at a single temperature or frequency and within a restricted bias voltage range. This work aims to determine the electrical modulus, conductivity, basic dielectric properties, and impedance properties of Al/p-Si (MS) interlayer structures grown by spin coating method (%0.5 Bi:ZnO) using *C/G-V* measurements over a wide voltage range ((−4V)–(+4V)) and wide frequency range (0.1–1 MHz). At the same time, it is to increase the performance of Au/p-Si (MS) structures with an interlayer %0.5 Bi:ZnO. However, as is known, at low frequencies, the contribution to the measured *C* and *G* values is quite high due to interface states and polarization. To minimize their influence, impedance measurements were carried out at sufficiently high frequencies.

Experimental procedures

The fabrication of Al/%0.5 Bi:ZnO/p-Si/Au (MIS) structures was carried out on a p-Si wafer that had a thickness of 300 μm, a < 100 > float-zone, and a resistivity of 1–10 cm-Ω. The wafer was polished on one side. The p-Si wafer was first cleaned in an ultrasonic bath using conventional cleaning technique (RC) before being processed for production. After that, deionized water was used to properly rinse it, and nitrogen gas was used to dry it. Subsequently, the sample was moved straight into the vacuum chamber, where a high-pure gold sample (%99.89) with a thickness of 150 nm was heated to evaporate using a high-vacuum metal evaporation system that was running at 10^{-6} Torr. It was then annealed at 500 °C in a nitrogen atmosphere to obtain a low-resistivity or good ohmic contact. The produced %0.5 Bi:ZnO solution was then grown as an interfacial layer on the front of the p-Si wafer using the spin-coating technique. To obtain zinc (0.1 M) and nickel (0.1 M) solutions, respectively, zinc acetate (Zn $(CH_3COO)_2$) and nickel chloride ($NiCl_2$) were separately dissolved in 15 mL of methoxy ethanol. In addition, a 0.4 M base solution was made by dissolving NaOH in 65 ml of methanol. Ethanolamine served as a stabilizer while 0.1 M zinc solution and 0.4 M base solution were separately agitated for 10 min at 500 rpm to synthesize ZnO and Bi. To create solid films, the coated films were heated to 50 °C for an hour on a hot plate. Using a Fytronix spin coater system, PCBM, a fullerene derivative, was applied to the front of the p-Si wafer for 30 s at 2000 rpm and 80 °C to further modify it. Attaining the best coating properties for the layer is contingent upon maintaining this temperature of 80 °C. It is possible to obtain a very uniform layer with improved substrate adherence under these specified circumstances. PCBM was coated and then dissolved in chlorobenzene. Lastly, in the same thermal evaporation apparatus, the same high-pure Al with a 1-mm diameter and 150-nm thickness was placed onto the %0.5 Bi:ZnO interlayer. A quartz crystal metal thickness meter was used to regulate the thickness of the rectifier Al rectifier/Schottky connections as well as the back side of the Au ohmic contacts and their deposition rates. The produced samples were put on a copper holder after thin silver-coated wires were used as the electrode connection system to conduct electrical measurements. To avoid external effects, characterization measurements (C-V and G/w-V measurements) were performed within the Fytronix cryostat at about 10^{-3} Torr using the Fytronix-FY-7000 characterization equipment. For data collection and processing, a software application with an IEEE-488 ac/dc converter card was utilized. Figure 1 shows the schematic representation of the Al/%0.5 Bi:ZnO/p-Si/Au structure.
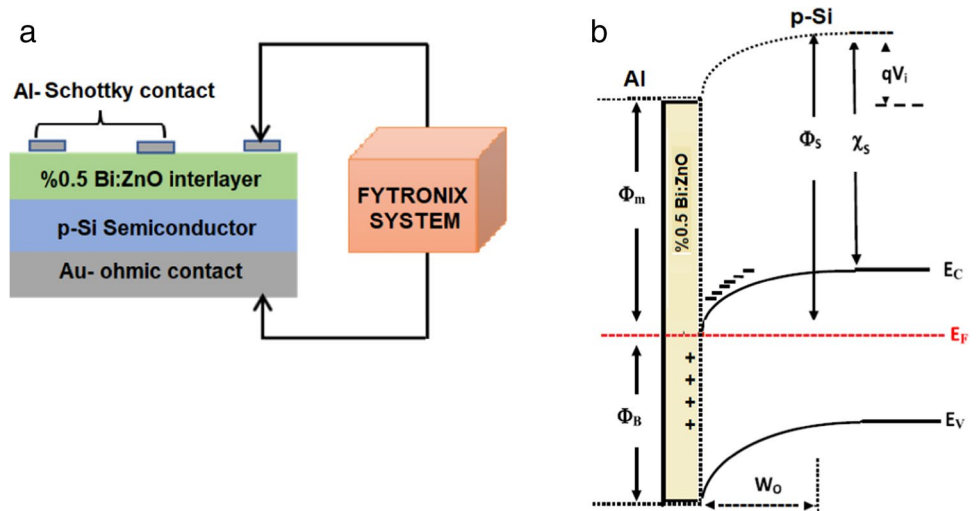
Results and discussions

The dielectric properties of the MIS structures are greatly affected by the frequency of the applied ac electric signal. This is caused by variations in the surface states' relaxation life as well as the applied ac signal's period ($T = 1/2\pi f$). The degree of polarization brought about by the applied electric field's influence on the dielectric materials is known as the dielectric permittivity ($\varepsilon^* = \varepsilon\prime - j\varepsilon\prime\prime$). Over a broad frequency range, it can be represented as a correlation of complex dielectric permittivity [38, 39], where $\varepsilon\prime$ and $\varepsilon\prime\prime$ are the real and imaginary components of ε^*, corresponding to the energy stored and lost during each field cycle. The real component, the dielectric constant ($\varepsilon\prime = \frac{C_m d_i}{\varepsilon_0 A}$), indicates how well the dipoles are aligned in the dielectric and quantifies the energy stored in the material because of the applied electric field. Conversely, the imaginary component is dielectric loss ($\varepsilon\prime\prime = \frac{G_m d_i}{\varepsilon_0 \omega A}$), which is the energy wasted in the dielectric due to frictional damping and which stops bound charge displacements from keeping up with the changing electric field [38, 40–42]. The values of both $\varepsilon\prime$ and $\varepsilon\prime\prime$ were calculated in the frequency range of 0.1–1 MHz and voltage range

of (−4V)–(+4V) at room temperature using the measured capacitance (Cm) and conductance (Gm). The quantity of energy lost as heat while the dielectric material is held under an electric field is provided by the value of tangent loss ($tan\delta = \frac{\varepsilon\prime\prime}{\varepsilon\prime} = \frac{G}{\omega C}$), when the $\varepsilon\prime$ and $\varepsilon\prime\prime$ are considered [40, 41, 43, 44].

Figures 2a and 3a show the changes of $\varepsilon\prime$ and $\varepsilon\prime\prime$ as a function of voltage in the frequency range 0.1–1 MHz, respectively. At low frequencies with considerable fluctuation, $\varepsilon\prime$ increases because the dipoles or space charges have enough time to reorient to the same direction as the external electric field. At the interface of the %0.5 Bi:ZnO/n-Si, these dipoles gather as a result of interfacial polarization (Maxwell–Wagner type polarization) caused by an external field [45]. Additionally, at lower frequencies, the trend of $\varepsilon\prime\prime$ nearly resembles that of $\varepsilon\prime$ due to the high mobility charge carriers present in the %0.5 Bi:ZnO interfacial layer. Through the interlayer material, these charges can travel forward or backward. Additionally, the movement and accumulation of charges at high frequencies lessen the creation of polarization, which lowers the dielectric loss. Furthermore, the frequency variations of $\varepsilon\prime$ and $\varepsilon\prime\prime$ can be seen in Figs. 2b and 3b for different applied bias voltages (0.1 to 0.5 V) in steps

Fig. 2 Plots of **a** voltage and **b** log (ω) dependent of $\varepsilon\prime$ the Al/%0.5 Bi:ZnO/p-Si/Au structure
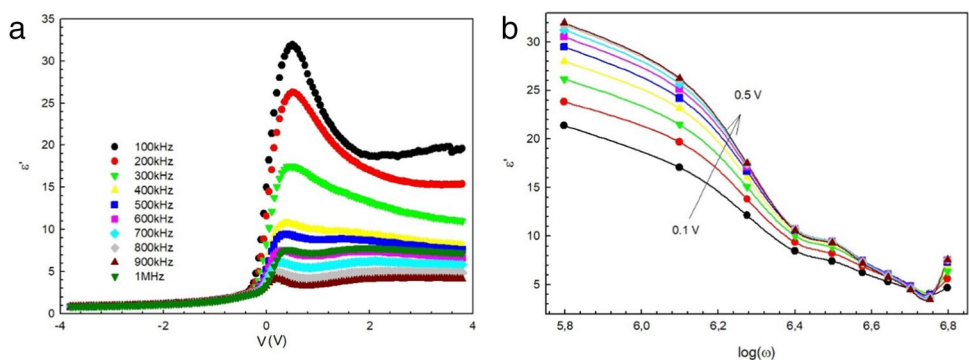
of 0.05 V, respectively. Figures 2b and 3b show that whereas ε' and ε'' values decrease with higher frequency, they both increase with an increase in positive voltage. The space-charge polarization was associated with the greater values of ε' and ε'' at lower frequencies. In addition to the effects of inhomogeneous barriers and electrode contact resistance, the polarization caused by accumulating dipoles or space charges at the interface is the cause of this trend in ε' and ε''.

A further measure of the manufactured structure's energy loss at a given frequency is the tangent dielectric loss (tanδ). The tanδ-V plots of the MIS capacitor in Fig. 4 clearly show a peak at all frequencies, which is related to the dielectric relaxation processes taking place in the interfacial layer. As the frequency increases, the peak position shifts towards higher voltages due to a distinct distribution of N_{ss} and

interfacial polarization. These findings demonstrate the dependence of dielectric characteristics on applied voltage, frequency, polarization processes and their relaxation durations, and interface traps. Because of the interlayer that is present at the M/S interface, they can store electric charges or energy, giving them capacitor-like properties.

To determine the polarization type and probable effective/dominant conduction mechanisms in the MIS capacitor, it is necessary to measure the ac electrical conductivity throughout a broad frequency and voltage range. Figure 5a and b show the semilogarithmic plots of σ_{ac}-V and σ_{ac}log(ω) of the MIS capacitor for different voltages in the accumulation region, respectively [39].

The hopping type of conduction in the materials, as seen in Fig. 5a–b, is supported by studies on electric modulus and
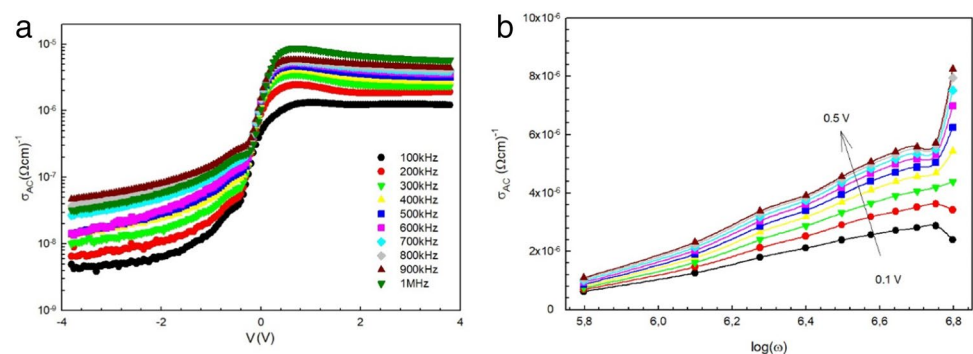

Fig. 3 Plots of **a** voltage and **b** log (ω) dependent of ε'' the Al/%0.5 Bi:ZnO/p-Si/Au structure
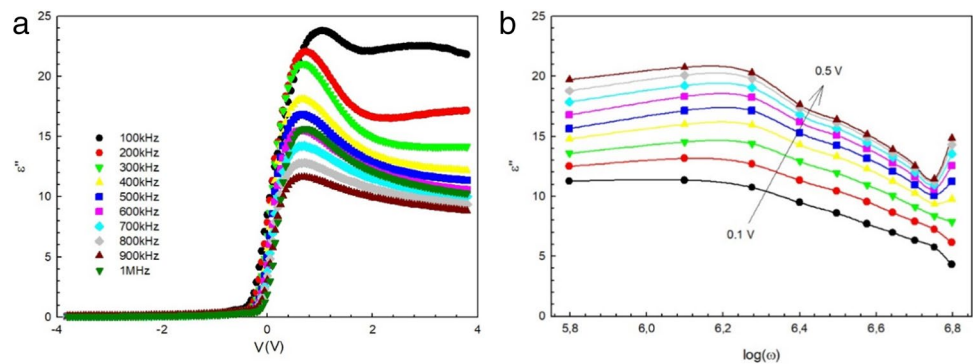
Fig. 4 Plots of **a** voltage and **b** log (ω) dependent of tanδ the Al/%0.5 Bi:ZnO/p-Si/Au structure
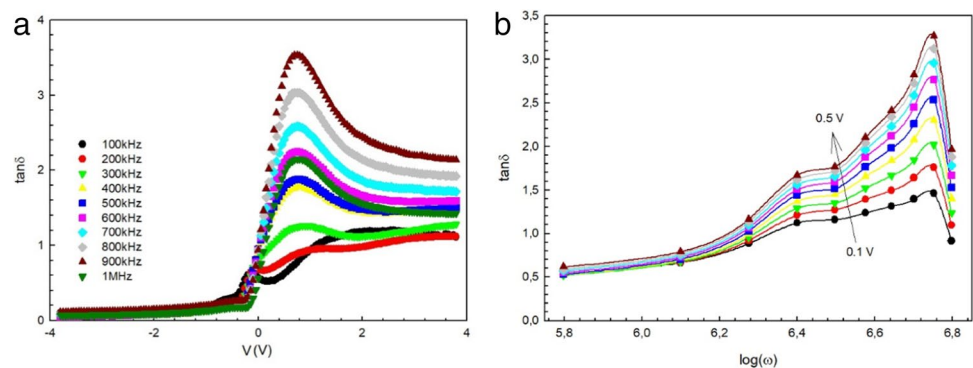
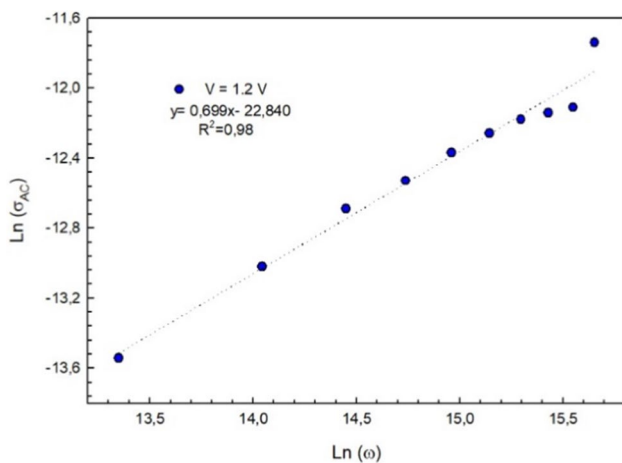**Fig. 5** Plots of **a** voltage and **b** log (ω) dependent of tanδ the Al/%0.5 Bi:ZnO/p-Si/Au structure

AC conduction, and it increases with increasing frequency and voltage because of frequency-dependent conduction. The possibility of space charges being released at higher frequencies could be supported by the greater σ_{ac} values observed at higher frequencies. Moreover, when the frequency rises, such behaviour may be linked to a decline in Rs. The hopping mechanism or conduction of mobile charge carriers helps explain this. Figure 5a makes it evident that there is a rise, nearly exponential at high frequencies, particularly in the forward bias area. This increase may be related to the dc conductivity. Ln(σ_{ac})-Ln (ω) curve has displayed linear behaviour, as seen in Fig. 6. The value of ac electrical conductivity at high frequency ($\sigma_{ac}(f) = A. \omega^s$) usually increases with increasing frequency as linearly at accumulation region. Here, A is a constant and s is the double logarithmic σ_{ac}-ω plot's slope. Slope values are often expected to fall between 0 and 1, which may provide details about the conduction process described in the literature. In this study, the slope of the double logarithmic σ_{ac}-ω plot shows good linear behaviour and so the value slope was found 0.699 which is lower than unity. This value of slope confirms that the Al/%0.5 Bi:ZnO/p-Si/Au structure has low resistivity ($\sigma = 1/\rho$) or high

Fig. 6 Frequency dependent Ln(σ_{ac})-Ln(ω) plot of the Al/%0.5 Bi:ZnO/p-Si/Au structure at 1.2 V

ac conductivity. This value of slope (= 0.699) shows that the conduction/charge transport mechanism may be occurred when electrons jump from one surface-state level or trap to another which is known as the relaxation model [40, 41].

The relaxation of the electric field in a thin interfacial layer at the M/S interface is generally explained by the electric modulus. There is yet another way to show the structure's dielectric response and uncover additional effects: the complex modulus analysis. The complex electric modulus ($M^* = 1/\varepsilon^* = M\prime + jM\prime\prime = \varepsilon\prime/(\varepsilon\prime^2 + \varepsilon\prime\prime^2) + j\varepsilon\prime\prime/(\varepsilon\prime^2 + \varepsilon\prime\prime^2)$) formalism of MIS structures is derived from the structures' dielectric properties [46–50]. $M\prime$ refers to the real component of complex modulus, and $M\prime\prime$ for the imaginary component.

Figures 7 and 8 show the $M\prime$ and the $M\prime\prime$ in relation to the voltage response and frequency for the Al/%0.5 Bi:ZnO/p-Si/Au structure. The value of $M\prime$ is practically in a decreasing trend when the applied bias voltage increases from the reverse to the forward area, as shown in Fig. 7a. On the other hand, as Fig. 7b illustrates, the value of $M\prime$ shows an increasing tendency for forward biases dependent on frequency. Due to electrons' limited mobility, this behaviour of $M\prime$ with frequency may contribute to conduction phenomena. As seen in Fig. 8a and b, the dielectric relaxation processes (Maxwell-Wenger type polarization) are represented by a peak in the $M\prime\prime$-V plots at around 0 V for each frequency. The unique distribution of N_{ss} localized at the p-Si/%0.5 Bi:ZnO interface causes the position of the peak to slide to forward bias voltages with increasing frequency [41]. The $M\prime\prime$-V plot's singular peak is the outcome of charge carriers moving great distances. We conclude that the Maxwell–Wagner type polarization is the cause of the inhomogeneity non-complex dielectric and electric modulus [38, 40].

Because different capacitive components result in different relaxation processes, the Cole–Cole plots are utilized to differentiate between them. Impedance spectroscopy (IS) is a useful technique for elucidating the electrical characteristics of materials. The MIS structure's $M\prime\prime$-$M\prime$ curve is displayed in Fig. 9 for three distinct frequency values (200 kHz, 500 kHz, and 1 MHz). It displays a semicircular arc that is sequential for all three frequency levels. The existence of this semicircular arc suggests that grains, not grain boundaries, are responsible
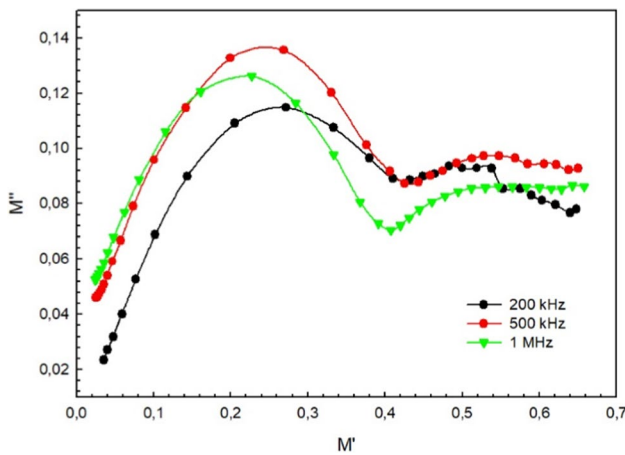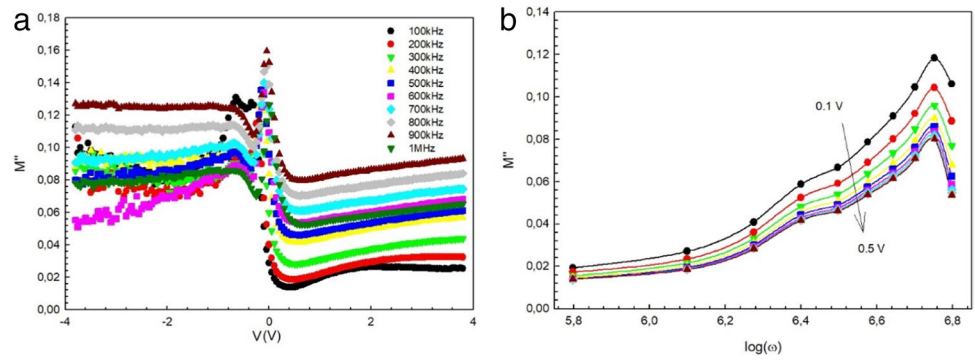
Fig. 7 Plots of **a** voltage and **b** log (ω) dependent of $M\prime$ the Al/%0.5 Bi:ZnO/p-Si/Au structure
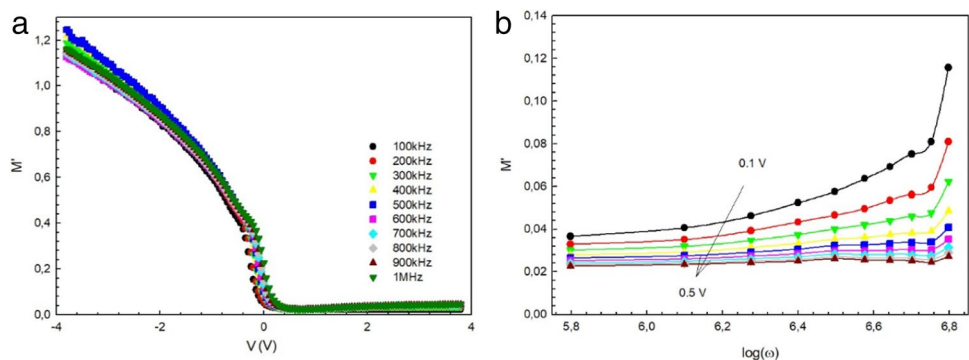
Fig. 8 Plots of **a** voltage and **b** log (ω) dependent of M″ the Al/%0.5 Bi:ZnO/p-Si/Au structure

Fig. 9 The curves of *M″-M′* of the Al/%0.5 Bi:ZnO/p-Si/Au structure

for the polarization mechanism in the interface layer. Furthermore, the *M″-M″* plot indicates the presence of overlapping semicircular arcs that exhibit a diminishing diameter as frequency increases. These arcs are attributed to contributions from the electrode-grain interface and the grain boundary in decreasing order of measurement frequency.

To learn more about the dielectric characteristics of interfacial materials, scientists employ a technique called complex impedance spectroscopy (IS). As a result, the complex impedance ($Z^* = \frac{1}{i\omega C_o \varepsilon^*} = Z' - jZ'' = \frac{\varepsilon''}{\omega C_o \left(\varepsilon'^2 + \varepsilon''^2 \right)} - j \frac{\varepsilon'}{\omega C_o \left(\varepsilon'^2 + \varepsilon''^2 \right)}$) can be used

to examine the materials'dielectric behaviour. The real component of complex impedance is denoted by Z′, and the imaginary component is denoted by Z″.

Figures 10a and 11a show the values of Z′ and Z″ in the frequency range of 0.1–1 MHz, respectively. Furthermore, the Z′ and Z″ variations in the voltage range of 0.1 to 0.5 V step by 0.05 V for the Al/%0.5 Bi:ZnO/p-Si/Au structure are displayed in Figs. 10b and 11b, respectively, in the frequency range of 0.1–1 MHz. Based on the Z′-Z″-V graphs, Z′ exhibits a steep decline at the same voltages as Z″, whereas Z′ shows a peak for all frequency values at a voltage of approximately 0 V because of stable loads and N_{ss}.

The impedance measurement can be used to calculate the phase angle ($\theta = tan^{-1}\left(\frac{Z''}{Z'} \right)$) between the capacitive current and the resistive current [51–53]. Figure 12 shows the phase angle profile's voltage dependence on the structure as well as the phase angle's invariant value close to 90° for the reverse bias voltage region. The pure capacitive behaviour of the structure is indicated by these consistent values of θ as 90° during the reverse bias voltage region. For every frequency value, the θ value rapidly decreases until it reaches its minimum value, about 0 V. Similar variations in temperature, voltage, and frequency have also been reported in several electronic devices having an organic interfacial layer in recent years [54–60].

In recently, research has focused on electrical transport and electric characteristics, relaxation processes, morphology, and crystal structure synthesis in some interlayer

Fig. 10 Plots of **a** voltage and **b** log (ω) dependent of Z′ the Al/%0.5 Bi:ZnO/p-Si/Au structure
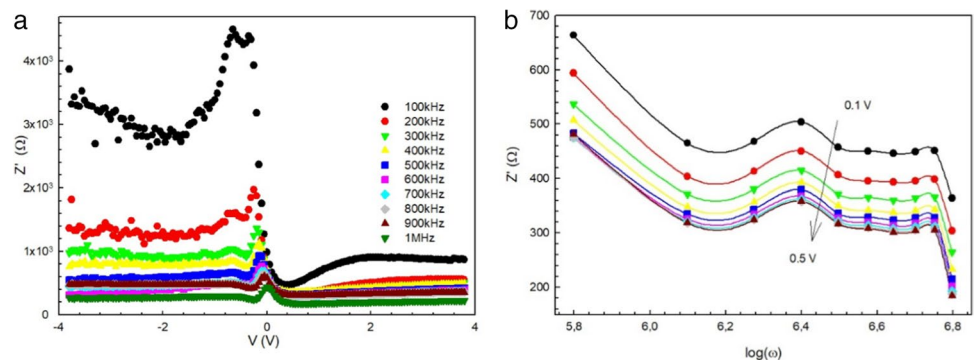
Fig. 11 Plots of **a** voltage and **b** log (ω) dependent of Z'' the Al/%0.5 Bi:ZnO/p-Si/Au structure
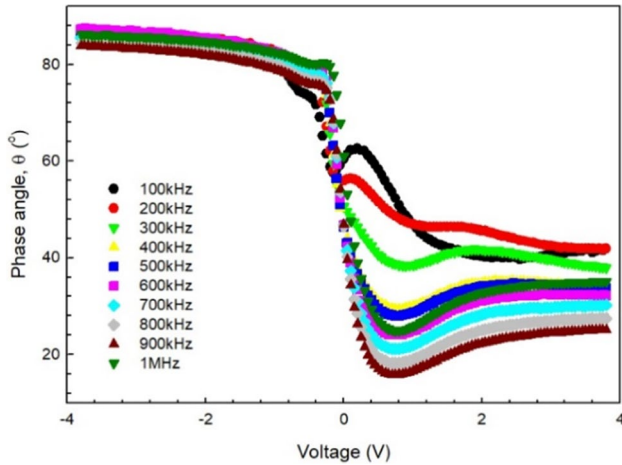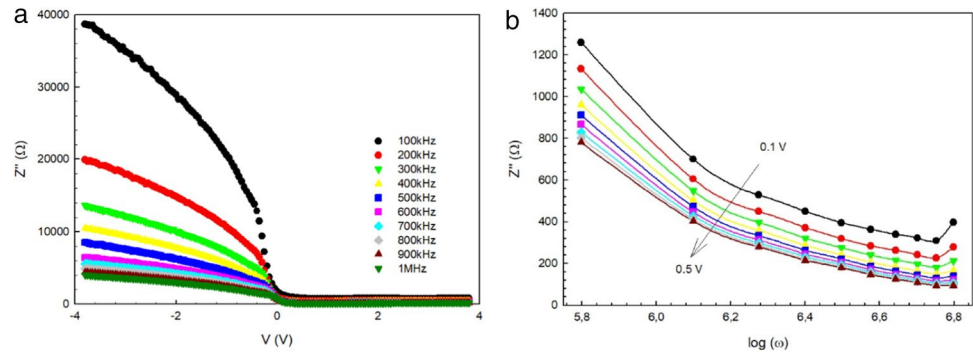
Fig. 12 The voltage dependence of phase angle (θ) for Al/%0.5 Bi:ZnO/p-Si/Au structure

composites, as well as defect characterization utilizing various approaches [61–67]. They indicated that the charge transport mechanism, hopping mechanisms, relaxation process, and electric and dielectric properties in the various materials or interfacial layer materials are considerably dependent on frequency, voltage or electric field, temperature, illumination, doping ratio, the thickness and homogeneity of interlayer, dislocations, or defects characteristics. As a result, in this study, experimental results also shown that the used (Bi:ZnO) interfacial layer has a high dielectric constant (~33) even at 100 kHz. This is quite high compared to classical MIS or MOS structures with an insulator/oxide interfacial layer. This means that the prepared structure can store many electronic charges or energy storage capacity like an ultra-capacitor.

Conclusion

In the present study, a wide frequency range of 0.1–1 MHz was studied using C/G-V measurements to examine the effects of voltage and frequency on the electric modulus,

ac electrical conductivity dielectric constant, dielectric loss, and tangent-loss of the Al/(%0.5 Bi:ZnO)/p-Si/Au (MIS) structures. It was discovered that all these characteristics were highly dependent on frequency and voltage. Examining how ε', ε'', and tanδ values vary with frequency and voltage leads to the conclusion that, because of the existence of N_{ss}, they exhibit frequency dependence in the depletion and accumulation regions and voltage dependence at low frequencies. The increased values of σ_{ac} seen at a higher frequency might indicate the possibility of space charge release at higher frequencies. Moreover, when the frequency rises, such behaviour may be linked to a decline in Rs. The hopping mechanism or conduction of mobile charge carriers helps explain this. The Ln(σ_{ac})-Ln (ω) curve exhibited a linear pattern. With a slope of 0.699, this plot indicates that the conduction mechanism could arise from electrons skipping from one surface-state level or trap to another, a process that is well-known to occur in relaxation models. The experimental results reveal a notable increase in the M' value as frequency rises, while M'' manifests a peak whose location shifts towards positive voltages with increasing frequency. The frequency-dependent alterations in M^{*}'s real and imaginary parts are attributed to the presence of Maxwell–Wagner polarization and a distinct arrangement of interface states at the Au/interlayer junction. These modifications are intricately associated with the inherent capacity of both interface states and dipoles to effectively trace the alternating current (AC) signal. Consequently, this behaviour results in the characteristic manifestation of a Cole–Cole curve in the M''-M' relationship. This curve signifies the occurrence of overlapping semicircular arcs with diminishing diameters at higher voltages, indicating contributions from the electrode-grain interface and grain boundaries at lower frequencies. Based on the Z'-Z''-V plots, Z' exhibits a dramatic decline in the same voltage area whereas Z' displays a peak for all frequency values at roughly 0 V voltage because of the stable charges and N_{ss}. However, the Z' and Z'' values also exhibit a drop that gets more frequent until it reaches its lowest and nearly constant value. The space charge polarization can be used to explain these frequency changes of Z' and Z''.

Declarations

Competing interests The authors declare no competing interests.

References

1. Gullu HH, Yildiz DE (2021) Capacitance, conductance, and dielectric characteristics of Al/TiO2/Si diode. J Mater Sci: Mater Electron 32:13549

2. Ulusoy M, Altındal Ş, Azizian-Kalandaragh Y, Özçelik S, Mirzaei-Kalar Z (2022) The electrical characteristic of an MIS structure with biocompatible minerals doped (brushite+monetite: PVC) interface layer, microelectron. Eng 258:111768

3. Karadeniz S, Yıldız DE (2023) Frequency dependent dielectric spectroscopy of Au/n-Si structure with stannic oxide (SnO2) interfacial layer. J Mater Sci: Mater Electron 34:1416

4. Büyükbaş-Uluşan A, AltındalYerişkin S, Tataroğlu A, Balbasi M, Azizian-Kalandaragh Y (2020) Dielectric, ac conductivity and electric modulus studies at MPS structure with (Cu2O-CuO)-doped PVA interfacial layer, optoelectron. Adv Mater Rapid Commun 14:256

5. Sevgili Ö, Taşçoıoğlu İ, Boughdachi S, Azizian-Kalandaragh Y, Altındal Ş (2019) Examination of dielectric response of Au/HgS-PVA/n-Si (MPS)structure by impedance spectroscopy method. Phys B Condens Matter 566:125

6. Bengi S, Yükseltürk E, Bülbül MM (2023) Investigation of electrical characterization of Al/HfO2/p-Si structures in wide temperature range. J Mater Sci: Mater Electron 34:189

7. Yu JH, Chestakov DA, Eggink HJ (2013) In-situ analysis of thermal properties of polymer composites by embedded LED temperature sensor. Microelectron J 44:1025–1028

8. Depas M, Van Meirhaeghe RL, Laflere WH, Cardon F (1992) A quantitative analysis of capacitance peaks in the impedance of Al/SiOx/p-Si tunnel diodes. Semicond Sci Technol 7:1476–1483

9. Prasad CV, Reddy MSP, Reddy VR, Park C (2017) Effect of annealing on chemical, structural and electrical properties of Au/Gd2O3/n-GaN heterostructure with a high-k rare-earth oxide interlayer. Appl Surf Sci 427:670–677

10. Szatkowski J, Sierański K (1992) Simple interface-layer model for the nonideal characteristics of the Schottky-barrier diode. Solid-State Electron 35:1013–1015

11. Nicollian EH, Goetzberger A (1965) MOS conductance technique for measuring surface state parameters. Appl Phys Lett 7:216–219

12. ErbilenTanrıkulu E, Taşçıoğlu İ (2023) Variation of the surface states and series resistance depending on voltage, and their effects on the electrical features of a schottky structure with CdZnO interface. J Electr Mater 52:2432–2440

13. Ocaya RO, Erol I, Al-Sehemi AG, Dere A, Al-Ghamdi AA, Yakuphanoglu F (2022) ZnO-doped PFPAMA: a novel transparent conducting polymer for fast photodiodes. J Mater Sci: Mater Electron. 33:24803–24818

14. OrkunTan S, Tasçıoglu I, Altındal Ş (2021) Frequency response of metal-semiconductor structures with thin-films sapphire interlayer by ALD technique. IEEE Trans Electron Devices 68:10

15. Paratap Reddy MS, Lee JH, Jang JS (2013) Frequency-dependent series resistance and interface states in Au/bio-organic/n-GaN Schottky structures based on DNA biopolymer. Synth Met 185:167–171

16. Cetinkaya HG, FeizollahiVahid A, Basman N, Demirezen S, ŞafakAsar Y, Altındal S (2023) On the wide range frequency and voltage dependence of electrical features and density of surface states of the Al/(Cu:DLC)/p-Si/Au Schottky diodes (SDs). J Mater Sci: Mater Electr. 34:822

17. Ulusoy M, Badali Y, Pirgholi-Givi G, Azizian-Kalandaragh Y, Altındal Ş (2023) The capacitance/conductance and surface state intensity characteristics of the Schottky structures with ruthenium dioxide-doped organic polymer interface. Synth Met 292:117243

18. Ersoz G, Yucedag I, Azizian-Kalandaragh Y, Orak I (2016) S¸Altındal, Investigation of electrical characteristics in Al/CdS-PVA/p-Si (MPS) structures using impedance spectroscopy method. IEEE Trans Electron Devices 63:2948–2955

19. Faraz SM, Khan HR, Shah W, UlWahab Q, Nur O et al (2021) Effect of annealing temperature on the interface state density of n-ZnO nanorod/p-Si heterojunction diodes. Open Phys 19:467–476

20. Ocak YS (2012) Electrical characterization of DC sputtered ZnO/p-Si heterojunction. J Alloy Compd 513:130–134

21. Çetinkaya HG (2018) Frequency and voltage dependent profile of dielectric parameters and electric modulus for Al/(HgS-PVA)/p-Si Capacitor via impedance spectroscopy method. J Nanoelectron Optoelectron 13:421–427

22. Faraz SM, Shah W, Alvi NUH, Nur O, Wahab QU (2020) Electrical characterization of Si/ZnO nanorod PN heterojunction diode. Adv Condens Matter Phys 1:1–9

23. Faten E, Al-Hazmi F (2018) Yakuphanoglu, Photoconducting and photovoltaic properties of ZnO:TiO2 composite/p-silicon heterojunction photodiode. SILICON 10:781–787

24. AksuCanbay C, Tataroğlu A, Dere A, Al-Sehemi AG, Karabulut A, Al-Ghamdih AA, Yakuphanoglu F (2021) Electrical, kinetic and photoelectrical properties of CuAlMnMg shape memory alloy/n-Si Schottky diode. J Alloys Compd 888:161600

25. Raship NA, Tawil SNM, Nayan N, Ismail K (2023) Effect of Al concentration on structural, optical and electrical properties of (Gd, Al) Co-Doped ZnO and its n-ZnO/p-Si (100) heterojunction structures prepared via co-sputtering method. Materials. 16:2392

26. Ulusoy M, Altındal S, Durmus P, Ozcelik S, Azizian-Kalandaragh Y (2021) Frequency and voltage-dependent electrical parameters, interface traps, and series resistance profile of Au/(NiS:PVP)/n-Si structures. J Mater Sci: Mater Electron 32:13693–13707

27. Yang D, Jonnalagadda R, Rogers BR, Hillman JT, Foster RF, Cale TS (1998) Texture and surface roughness of PRCVD aluminum films. Thin Solid Films 332

28. Kang DJ, Kim JS, Jeong SW, Roh Y, Jeong SH, Boo JH (2005) Structural and electrical characteristics of R.F. magnetron sputtered ZnO films. Thin Solid Films 475:160–165

29. Bülbül MM, Bengi S, Dökme İ, Altındal Ş, Tunç T (2010) Temperature dependent capacitance and conductance-voltage characteristics of Au/polyvinyl alcohol(Co, Zn)/n-Si Schottky diodes. J Appl Phys 108:034517

30. Kartci A, Vancik S, Prasek J, Hrdy R, Schneider M, Schmid U, Hubalek J (2022) Comparison of on-chip MIS capacitors based on stacked HfO2/Al2O3 nanolaminates. Appl Mater Today 33:104664

31. Baltakesmez A, Güzeldir B, Sağlam M, Biber M (2021) Interpretation of the I-V, C–V and G/ω-V characteristics of the Au/ZnS/n-GaAs/In structure depending on annealing temperature. Physica B 611:412801

32. Gumus I, Aydogan S (2021) The electrical and dielectric properties of the magnetite nanoparticles supported graphene-oxide/n-Si MOS type device that operates across a wide temperature range. Sensors Actuators A 331:112989

33. Yıldız DE, Tataroglu A (2023) Analysis of dielectric, impedance and electrical properties of interfacial layer: AlN. J Mater Sci: Mater Electron 34:1057

34. Cova P, Singh A, Masut RA (1997) A self-consistent technique for the analysis of the temperature dependence of current–voltage and capacitance–voltage characteristics of a tunnel metal-insulator-semiconductor structure. J Appl Phys 82:5217

35. Güçlü ÇŞ, Özdemir AF, Aldemir DA, Altındal Ş (2021) The reverse bias current–voltage–temperature (I–V–T) characteristics of the (Au/Ti)/Al2O3/n-GaAs Schottky barrier diodes (SBDs) in temperature range of 80–380 K. J Mater Sci: Mater Electron 32:5624–5634

36. Chattopadhyay P, Raychaudhuri B (1993) Frequency dependence of forward capacitance-voltage characteristics of Schottky barrier diodes. Solid State Electron 35:605

37. Demirci A, Çetinkaya HG, Durmuş P, Demirezen S, Altındal Ş (2023) Optoelectronic characterization of Bi-doped ZnO nanocomposites for Schottky interlayer applications. Physica B 670:415338

38. Kaya A, Zeyrek S, San SE, Altindal Ş (2013) Electrical and dielectric properties of Al/p-Si and Al/perylene/p-Si type diodes in a wide frequency range. Chinese Phys. B 23:018506

39. Demir GE, Yücedağ İ, Azizian-Kalandaragh Y, Altındal Ş (2018) J Electron Mater 47:6600

40. Chelkowski A (1980) Dielectric physics. Elsevier, Amsterdam

41. Popescu M, Bunget I (1984) physics of solid dielectrics. Elsevier, Amsterdam

42. Lapa HE, Kökce A, Özdemir AF, Uslu İ, Altindal Ş (2018) A comparative study on dielectric behaviours of Au/(Zn-doped PVA)/n-4H-SiC (MPS) structures with different interlayer thicknesses using impedance spectroscopy methods. Bullet Mater Sci 41:82

43. Symth CP (1955) Dielectric behaviour and device. McGraw-Hill, New York

44. Vera Daniel V (1967) Dielectric relaxation (Academic Press, London)

45. Taşçıoğlu İ, Sevgili Ö, Azizian-Kalandaragh Y, Altındal Ş (2020) Frequency-dependent admittance analysis of Au/n-Si structure with CoSO4-PVP interfacial layer. J Electron Mater 49:3720–3727

46. Sevgili Ö, Taşçıoğlu İ, Boughdachid S, Azizian-Kalandaraghd Y, Altındal Ş (2019) Examination of dielectric response of Au/HgS-PVA/n-Si (MPS) structure by impedance spectroscopy method. Physica B 566:125

47. Altındal Ş, Barkhordari A, Azizian-Kalandaragh Y, Çevrimli BS, Mashayekhi HR (2022) Dielectric properties and negative-capacitance/dielectric in Au/n-Si structures with PVC and (PVC:Sm2O3) interlayer. Mater Sci Semicond Process 147:106754

48. Sevgili Ö, Azizian-Kalandaragh Y, Altındal Ş (2020) Frequency and voltage dependence of electrical and dielectric properties in metal-interfacial layer-semiconductor (MIS) type structures. Physica B 587:412122

49. Sevgili Ö (2021) The investigation of the complex dielectric and electric modulus of Al/MgSi/p-Si Schottky diode and its AC electrical conductivity in a wide frequency range. Turk J Phys 45:159

50. Azizian-Kalandaragh Y, Badali Y, Jamshidi-Ghozlu MA, Hanife F, Ozçelik S, Altındal S, Pirgholi-Givi G (2023) The temperature-dependent dielectric properties of the Au/ZnO-PVA/n-Si structure. Physica B 650:414495

51 Demirezen S, Yerişkin SA (2021) Frequency and voltage-dependent dielectric spectroscopy characterization of Al/(Coumarin-PVA)/p-Si structures. J Mater Sci Mater Electron 32:25339

52. Akbaş AM, Tataroğlu A, Altındal Ş, Azizian-Kalandaragh Y (2021) Frequency dependence of the dielectric properties of Au/(NG:PVP)/n-Si structures. J Mater Sci Mater Electron 32:7657

53. Asar YŞ, Sevgili Ö, Altındal Ş (2023) Investigation of dielectric relaxation and ac conductivity in Au/(carbon nanosheet-PVP composite)/n-Si capacitors using impedance measurements. J Mater Sci: Mater Electron 34:893

54. Güneşer MT, Elamen H, Badali Y, Altındal Ş (2023) Frequency dependent electrical and dielectric properties of the Au/(RuO2:PVC)/n-Si (MPS) structures. Physica B 657:414791

55 Vahid FA, Alptekin S, Basman N, Ulusoy M, ŞafakAsar Y, Altındal Ş (2023) The investigation of frequency dependent dielectric properties and ac conductivity by impedance spectroscopy in the Al/(Cu-doped Diamond Like Carbon)/Au structures. J Mater Sci: Mater Electron 34:1118

56. Karadaş S, Yerişkin SA, Balbaşı M, Azizian-Kalandaragh Y (2021) Complex dielectric, complex electric modulus, and electrical conductivity in Al/(Graphene-PVA)/p-Si (metal-polymer-semiconductor) structures. J Phys Chem Solids 148:109740

57. Bilkan Ç, Azizian-Kalandaragh Y, Altındal Ş, Shokrani-Havigh R (2016) Frequency and voltage dependence dielectric properties, ac electrical conductivity and electric modulus profiles in Al/Co3O4-PVA/p-Si structures. Physica B: Phys Condens Matter 500:154

58. Karaoğlan N, Tecimer HU, Altındal Ş, Bindal C (2019) Dielectric characterization of BSA doped-PANI interlayered metal–semiconductor structures. J Mater Sci: Mater Electron 30:14224

59. Azizian-Kalandaragh Y, Yücedağ İ, ErsözDemir G, Altındal Ş (2021) Investigation of the variation of dielectric properties by applying frequency and voltage to Al/(CdS-PVA)/p-Si structures. J Mol Struct 1224:129325

60. Yerişkin SA, Balbaşı M, Tataroğlu A (2016) Frequency and voltage dependence of dielectric properties, complex electric modulus, and electrical conductivity in Au/7% graphene doped-PVA/n-Si (MPS) structures. J Appl Polym Sci 133:43827

61. Ram R, Bhattacharya S (2023) Mixed ionic-electronic transport in Na2O doped glassy electrolytes: promising candidate for new generation sodium ion battery electrolytes. J Appl Phys 133:145101

62. Halder P, Bhattacharya S (2023) Debye to non-debye type relaxation in MoO3 doped glassy semiconductors: a portrait on microstructure and electrical transport properties. Physica B 648:414374

63 Das AS, Roy M, Roy D, Bhattacharya S, Nambissan PMG (2018) Identification of defects in the transition metal oxide-doped glass nanocomposite xV2O5–(1–x)(0.05MoO3–0.95ZnO) using positron annihilation spectroscopy and other techniques. J Non-Crystalline Solids 482:52–62

64. Bhattacharya S, Acharya A, Biswas D, Das AS, Singh LS (2018) Conductivity spectra of lithium ion conducting glassy ceramics. Physica B 546:10–14

65. Das AS, Roy M, Biswas D, Kundu R, Acharya A, Roy D, Bhattacharya S (2018) Ac conductivity of transition metal oxide doped glassy nanocomposite systems: temperature and frequency dependency. Mater Res Express 5(9):095201

66. Das AS, Roy M, Roy D, Bhattacharya S, Nambissan PMG (2018) Defects characterization and study of amorphous phase formation in xV2O5-(1–x) Nd2O3 binary glass nanocomposites using positron annihilation and correlated experimental techniques. J Alloy Compd 753:748–760

67. Das AS, Roy M, Roy D, Kar T, Rath S, Bhattacharya S (2017) Investigations of microstructure and dc conductivity of V2O5-Nd2O3 glass nanocomposites. ChemistrySelect 2(34):11273–11280